JOURNAL OF MATERIALS SCIENCE 29 (1994) 3969–3978

Molecular weight and polydispersity effects on interdiffusion at the interface between polystyrene and poly(vinyl methyl ether)

E. JABBARI, N. A. PEPPAS*
School of Chemical Engineering, Purdue University, West Lafayette, IN 47907, USA

Time dependence and the effect of polystyrene (PS) and poly(vinyl methyl ether) (PVME) molecular weight and polydispersity on interdiffusion at the interface of PS and PVME were investigated with attenuated total reflection infrared spectroscopy (ATR–FTIR). The time dependence of interdiffusion was studied by varying the thickness of the slow-diffusing component, PS, and the results were analysed using a combination of Fickian and Case II models. PS samples with molecular weights ranging from 1.0×10^5 to 3.0×10^6, above the entanglement molecular weight, were used to study the effect of molecular weight on interdiffusion. PS samples with controlled polydispersity ranging from 1.1–3.0 were prepared using a trimodal distribution constructed from monodisperse PS samples. The polydispersity of the PS samples was controlled by varying the number average molecular weight of the distributions while keeping the weight average molecular weight constant. To study the effect of PVME molecular weight and molecular weight distribution on interdiffusion, PVME was fractionated three times from an aqueous solution to increase its molecular weight from 9.9×10^4 to 1.7×10^5 and reduce its polydispersity index from 2.1 to 1.4, respectivley.

1. Introduction

In general, adhesion at polymer–polymer interfaces affects the mechanical properties of polymers near these interfaces [1]. This process, in turn, influences various phenomena such as welding of polymer interfaces and lamination of composites.

Microscopic adhesion is related to the intermolecular interactions at the interface and depends exclusively on the interfacial characteristics [2]. On the other hand, macroscopic adhesion is related to the irreversible processes at the interface and is affected by specimen geometry and measurement techniques. Therefore, the adhesive strength of a bond is the sum of the microscopic forces (reversible work) and macroscopic adhesion (irreversible work).

Polymer–polymer adhesion may be interpreted by the theories of adsorption [3], wetting [4], diffusion [5, 6], fracture [1], kinetic [7], and by mechanical interlocking [8]. Of these theories, the diffusion theory of Voyutskii [5] is of particular interest to us. After intimate contact is established between two polymer films, adhesion takes place by interdiffusion of polymer segments across the interface. The extent of interdiffusion and chain interpenetration depends on the compatibility between the two polymers. For compatible polymers the interface thickness is of the order of micrometres, whereas for incompatible polymers it is of the order of ångströms. It has been shown [9] that the extent of interdiffusion is directly proportional to the Flory–Huggins interaction parameter between the two polymers.

Interdiffusion in homopolymers, otherwise known as polymer healing, has been studied extensively with techniques such as neutron scattering [10], forward recoil spectrometry [11], Rutherford backscattering [12], and secondary ion mass spectrometry [13]. These techniques have shown unequivocal evidence for interdiffusion and chain interpenetration at polymer–polymer interfaces. In particular, Rutherford backscattering spectrometry [12] has been used to show movement of the interface toward the faster diffusing component at a polystyrene (PS) and deuterated PS (d-PS) interface with different molecular weights. The interface movement was of the order of 10 nm depending on the difference between the two molecular weights.

This interface movement has also been observed for partially compatible polymers such as PS and poly(styrene-co-4-bromostyrene) [14]. When the two polymers were contacted and annealed in the two-phase region, the interface shifted during equilibration to two phases corresponding to the binodal concentrations. This indicated that the phase diagram as well as the physical properties of the two polymers significantly influence the diffusion process and the concentration profile across the polymer–polymer interface. The interface movement was of the order of 50 nm depending on the binodal concentrations.

*Author to whom all correspondence should be addressed.

0022–2461

Recent results from Sauer and Walsh [15] and our laboratory [16] have shown that for polymer interfaces with dissimilar properties, the faster diffusing component swells the slower diffusing component prior to interdiffusion across the interface below and above the T_g of the slow-diffusing component. These results were obtained using a polymer pair consisting of PS as the slowly diffusing component with a glass transition temperature, T_g, 101 °C and poly(vinyl methyl ether) (PVME) as the fast diffusing component with $T_g = -27$ °C. The temperature range of the experiment was from 85–105 °C spanning temperatures below and above the T_g of PS.

The PS and PVME pair has been used extensively as a model to study adhesion at glassy and rubbery interfaces with applications in rubber-toughened polymer composites. For example, in lamination of composites, the polymer bilayer is annealed for a specified period of time at temperatures near the T_g of the two polymers to improve their interfacial adhesion. The temperature and duration of the annealing process directly affect the interfacial thickness and the adhesive strength of the glassy–rubbery interface.

The results of interdiffusion at the interface of PS and PVME were previously analysed with Fickian and Case-II models [17]. At 105 °C corresponding to 5 °C above the T_g of PS, the concentration profiles had 20% non-Fickian component. On the other hand, at 85 °C corresponding to 15 °C below the T_g of PS, the concentration profiles had 70% non-Fickian component. These are the first data exhibiting Case-II diffusion for diffusion at polymer–polymer interfaces above the entanglement molecular weight for below and above the T_g of the slow-diffusing component.

The effect of temperature on interdiffusion at PS–PVME interface was previously investigated by us [18]. These results showed that PVME swelled PS and this swelling could be characterized by an interface velocity. The relaxation time for the swelling process was determined from the interface velocity and it was controlled by the relaxation time of the slow-diffusing component, PS.

The objective of this work was to investigate the effect of molecular weight (MW) and molecular weight distribution (MWD) of PS and PVME on interdiffusion at the interface of PS–PVME below and above the T_g of the slow-diffusing component. A technique based on attenuated total reflection infrared spectroscopy, (ATR–FTIR), was used for quantitative analysis of interdiffusion at the PS–PVME interface.

2. Experimental procedure

2.1. Sample preparation

Polystyrene samples with weight average molecular weights, $\overline{M_w}$, of 1.5×10^4, 3.0×10^4, 1.05×10^5, 4.7×10^5, 8.5×10^5, and 3.0×10^6 and polydispersity indices of less than 1.06, were obtained from Pressure Chemical Co. (Pittsburg, PA) as primary standards. Poly(vinyl methyl ether) was obtained from Scientific Polymer Products (Ontario, NY) as a secondary standard with $\overline{M_w}$ of 9.9×10^4 and polydispersity index of 2.10. Gel permeation chromatography analysis of the two polymers indicated that no additives were present.

An FTIR spectrometer (Nicolet 800, Madison, WI) with an ATR accessory (Connecticut Instruments, Boston, MA) was used for the interdiffusion studies in the configuration shown in Fig. 1. The ATR crystal was germanium of 5 cm length, 1 cm width, and 2 mm thickness. Polystyrene films were cast from *p*-xylene or toluene solution on an ATR crystal with a spin coater (model 1-EC101D-R485, Photo-Resist Spinners, Garland, TX) at 250 r.p.m. For monodisperse PS samples with $\overline{M_w}$ of 1.05×10^5, 8.5×10^5, and 3.0×10^6, the solution concentration with 5.0%, 2.5%, and 1.5%, respectively. The concentration of PS was varied to control the solution viscosity for spin casting. For trimodal PS samples, the solution concentration was constant at 5.0%. The PS film was dried in a controlled atmosphere at 25 °C for at least 24 h, then *in vacuo* at 25 °C for 24 h, followed by *in vacuo* at 115 °C for 1 h to remove any residual solvent in the film. The film was then annealed at 115 °C for at least 12 h to remove solvent and minimize molecular orientation resulting from the spinning process. The thickness of the PS film was measured with a profilometer (alpha-step 200, Tencor Instruments, Mountain View, CA).

PVME was cast directly on PS films from a 10 wt % isobutanol solution using a spin coater at 250 r.p.m. The PVME film was dried at 25 °C for 24 h and then *in vacuo* at room temperature for 24 h to remove residual water. Because the T_g of PVME is below room temperature, further drying at higher temperatures was not necessary. The thickness of the PVME film was measured by casting a PVME film on a microscope slide with the same dimensions as the ATR crystal and under the same spinning conditions. The film was dired at 25 °C for 24 h and then *in vacuo* at room temperature for 24 h to remove residual water. The glass slide was weighed before and after the PVME film was cast. The thickness of the PVME film was 6.6 μm.

2.2. Preparation of PS samples with controlled polydispersity

Polydisperse PS samples were prepared using a trimodal distribution constructed from monodisperse PS samples with $\overline{M_w}$ of 1.5×10^4, 1.05×10^5, and 4.7×10^5. The polydispersity index of the samples were

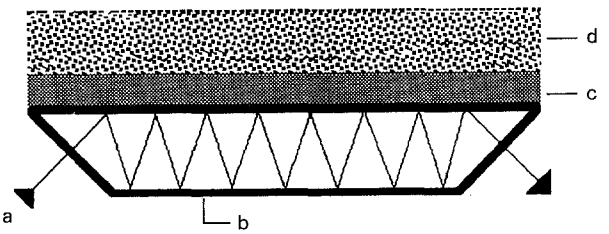

Figure 1 ATR assembly for *in situ* measurement of polymer–polymer interdiffusion. a, Infrared light beam; b, ATR crystal; c, PS layer; d, PVME layer.

controlled by varying the number average molecular weight of the distributions while keeping the weight average molecular weight constant. The weight per cent of each monodisperse polymer for preparing polydisperse samples with a trimodal distribution is given in Table I. For example, a PS sample with polydispersity index of 2.0 was constructed using a trimodal distribution with 16.7, 79.2, and 4.1 wt % monodisperse PS with $\overline{M_w}$ of 1.5×10^4, 1.05×10^5, and 4.7×10^5, respectively.

2.3. Fractionation of PVME

PVME was fractionated from water solution to reduce its molecular weight and polydispersity. PVME dissolves in water at 25 °C but it phase-separates above 37 °C. A 10% aqueous solution of as-received PVME with $\overline{M_w}$ of 9.9×10^4 and polydispersity index of 2.10 was allowed to equilibrate at 37 °C to form two phases. One phase was rich in PVME and the other phase rich in water and low molecular weight PVME. The PVME phase was separated from the water phase by decanting off the latter and this process was repeated three times to separate the lower molecular weight fraction of PVME. The fractionated PVME was analysed by GPC to determine its molecular weight and polydispersity index.

Molecular weight distribution analysis was carried out with a GPC system (model 6000A, Waters Associates, Milford, MA) with tetrahydrofuran as the solvent and μStyragel® columns with 10^5, 10^4, 10^3, 10^2 nm pore sizes and 1 ml min^{-1} flow rate. The $\overline{M_w}$ of the fractionated sample was calculated from the chromatogram using a standard calibration curve constructed from monodisperse PS samples. The polydispersity index was determined from the chromatogram width and the slope of the universal calibration curve using a method described by Gorbunov *et al.* [18]. The chromatogram width was adjusted for instrumental broadening by subtracting the variance of a monodisperse PS sample from the variance of the fractionated PVME sample. The fractionated PVME sample had a $\overline{M_w}$ and polydispersity index of 1.7×10^5 and 1.4, respectively.

2.4. Thermal analysis of the PS–PVME blends

Differential scanning calorimetry (DSC 2910, TA Instruments, Willmington, DE) was used to measure the T_g of PS and its blends with PVME. Blends of PS and PVME with known compositions ranging from 0%–100% PS by weight were cast in Petri dishes from a 1% solution in toluene. Toluene is a compatible solvent for PS as well as PVME. The films were dried in a controlled atmosphere at 25 °C for at least 24 h, then dried *in vacuo* at 25 °C for 24 h. The films were annealed at 105 °C for at least 12 h to ensure complete mixing of PS and PVME. The lower critical solution temperature of the PS– PVME blend with PS $\overline{M_w} = 1.0 \times 10^5$ and PVME with $\overline{M_w} = 9.9 \times 10^4$ with polydispersity index of 1.05 and 2.1, respectively, is 125 °C [19]. Therefore, the annealing temperature of 105 °C is well within the one-phase region of the PS–PVME phase diagram. The DSC of the blends were carried out at 5 °C min^{-1} under ambient conditions.

A thermogravimetric analyser (Hi-Res TGA 2950, TA Instruments, Wilmington, DE) was used to study the degradation behaviour of PVME and its blends with PS as a function of temperature. In a typical experiment, a sample was equilibrated to the desired temperature for degradation studies and the weight loss was recorded as a function of time under ambient conditions.

TABLE I. Composition of trimodal distribution sample constructed from monodisperse PS to examine the effect of PS molecular weight distribution

PS molecular weight, $\overline{M_w}$ (g mol^{-1})	PS (wt %)		
	PI = 1.1	PI = 2.0	PI = 3.0
1.5×10^4	0.0	16.7	34.4
1.05×10^5	100.0	79.2	57.1
4.7×10^5	0.0	4.1	8.5

2.5. Attenuated total reflection infrared spectroscopy

The use of ATR–FTIR for interdiffusion studies at polymer–polymer interfaces was described previously [16]. Briefly, the infrared beam enters the ATR crystal from one of the side faces. If the refractive index of the crystal is higher than the PS and the incident angle of the beam is higher than a critical angle then the infrared beam is totally reflected at the crystal/PS interface and the beam travels inside the crystal and exits from the other side face. However, due to diffraction at the crystal/polymer interface, a small fraction of the beam penetrates into the PS layer and is absorbed by PS [20]. The fraction of the beam which is absorbed gives rise to absorption bands in the ATR spectrum and is used to monitor the concentration of each component within the penetration depth in the polymer layer.

In a typical experiment, a PS film was cast by spin coating from *p*-xylene solutions on a germanium crystal. The PS film was dried in a controlled atmosphere to remove any residual solvent. The PVME was spin cast directly on the PS film from isobutanol solution to ensure molecular contact at the PS–PVME interface. The assembly consisting of the ATR crystal, the two polymer films, and the heating unit was heated to the desired interdiffusion temperature and the ATR–FTIR spectrum was collected *in situ* with 128 averaged scans and a resolution of 4 cm^{-1}. The spectra were recorded using a Globar (mid-infrared) light source with potassium bromide as the beam splitter and mercury cadmium telluride (MCT) detector, cooled to liquid nitrogen temperature. No polarization was used for the light source. The end-face angle of the ATR crystal and the optical angle of the infrared beam were 45°.

3. Analysis of results

3.1. Spectral analysis

Previously we discussed [16] the ATR–FTIR spectrum of PS and PVME in the high-frequency region and the assignment of each absorption band. The ATR–FTIR spectrum of a 50/50 wt/wt PS/PVME in the high-frequency region from 2700–3200 cm^{-1} is shown in Fig. 2. The PVME band at 2820 cm^{-1} and the PS bands at 2850 and 3030 cm^{-1} were used for quantitative analysis of the PS/PVME spectra.

Time evolution of the ATR–FTIR spectrum for interdiffusion in the PS–PVME pair at 105 °C is shown in Fig. 3. The absorbance scale corresponds to the spectrum at zero interdiffusion time. The other spectra were shifted by 0.015 absorbance units for visual clarity. Spectra 1–5 correspond to 0, 0.5, 1.0, 1.5, and 2.0 h interdiffusion time, respectively. For quantitative analysis, the PS–PVME spectrum was deconvoluted to relate the area under the three peaks to PS and PVME mole fractions. The deconvolution program uses the Levenberg–Marquardt fitting routine to fit the experimental convoluted absorbance data to a set of calculated Gaussian or Lorentzian peaks [16]. The best fit was obtained with a 50% Lorentzian and 50% Gaussian peak composition.

To relate the molar fraction of PVME to the relative absorbance of PVME and PS, a calibration curve was required. Blends of PS and PVME with known composition ranging from 10%–90% PS by weight were cast on a ZnSe crystal from a 1% solution in toluene at 250 r.p.m. The area under the peak was determined by deconvoluting the original spectrum. The area of the PVME band at 2820 cm^{-1}, the PS bands at 2850 and 3030 cm^{-1} were used to calculate the relative absorption of PVME and PS.

3.2. ATR–FTIR cumulative concentration

The relative intensity of infrared radiation decreases exponentially as a function of distance away from the crystal surface and is characterized by the penetration

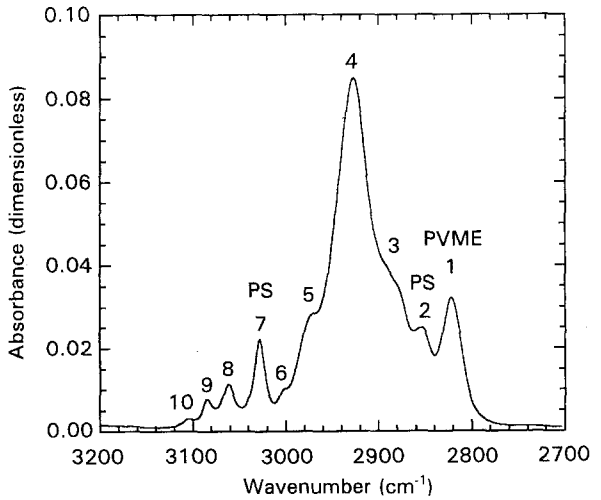

Figure 2 ATR–FTIR spectrum of a 50/50 wt/wt PS–PVME mixture in the high-frequency region. The peak frequencies 1–10 are 2820, 2850, 2880, 2930, 2975, 3000, 3030, 3060, 3085, and 3105 cm^{-1}, respectively.

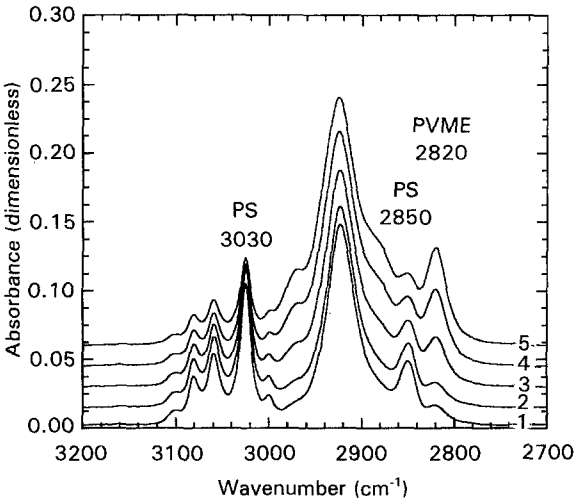

Figure 3 Time evolution of ATR–FTIR spectra for interdiffusion in a PS–PVME pair at 105 °C. The PS and PVME $\overline{M_w}$ were 1.05 × 10^5 and 9.9 × 10^4 with polydispersity indices of 1.06 and 2.10, respectively. The PS film was spin cast on a germanium crystal at 250 r.p.m. from a 5% *p*-xylene solution. The PVME film was spin cast on the PS film at 250 r.p.m. from a 10% isobutanol solution. The PS and PVME film thickness were 0.7 and 6.6 μm, respectively. The absorbance scale corresponds to spectrum 1 and the other spectra were shifted by 0.015 absorbance units. Spectra 1–5 correspond to 0.0, 0.5, 1.0, 1.5, and 2.0 h interdiffusion time, respectively

depth of the radiation within the polymer film. This exponential decrease has to be considered in order to compare the experimental results with model predictions. For an interdiffusion time, t, the mole fraction of PVME from the model, c_{PV}, at distance z was multiplied by its corresponding relative intensity and it was integrated over the penetration depth. This process was repeated for each interdiffusion time to give the cumulative concentration of PVME, $Q(t)$, versus time as given by

$$Q(t) = \frac{\int_0^\infty c_{PV}(z, t)\, I_{rel}(z)\, dz}{\int_0^\infty I_{rel}(z)\, dz} \quad (1)$$

where

$$I_{rel} = e^{-z/d_p} \quad (2)$$

and I_{rel} is the infrared intensity relative to the intensity at the interface, z is the distance from the crystal/polymer interface in the polymer layer, and d_p is the penetration depth of infrared radiation in the polymer medium. The penetration depth for germanium crystal with end-face and an optical angle of 45° is 0.114 μm for a PS–PVME pair and 3000 cm^{-1} IR frequency.

3.3. Fickian and Case II models

The experimental PVME cumulative concentration were analysed using a combination of Fickian and Case II models to obtain the interdiffusion coefficient and the interface velocity. The interdiffusion system consists of a PS layer with thickness δ_1, and a PVME layer with thickness δ_2 on a ATR crystal, as shown in Fig. 1. The interdiffusion direction is along the z-axis

which is perpendicular to the PS–PVME interface with the origin at the crystal/PS interface. The PVME concentration profile across the interface as a function of distance and time was derived elsewhere [16] for Fickian diffusion

$$c_{PV}(z,t) = 1 - \frac{c_0}{2}\sum_{n=-\infty}^{n=+\infty}\left\{\mathrm{erf}\left[\frac{\delta_1 + 2n(\delta_1+\delta_2) - z}{2(Dt)^{1/2}}\right] + \mathrm{erf}\left[\frac{\delta_1 + 2n(\delta_1+\delta_2) + z}{2(Dt)^{1/2}}\right]\right\} \quad (3)$$

where c_{PV} is the molar concentration of PVME, D is the interdiffusion coefficient, z is the distance across the interface, t is the interdiffusion time, and c_0 is the initial molar concentration of PVME. Substituting for c_{PV} from Equation 3 in Equation 1 gives the Fickian component of the PVME cumulative concentration, Q_F.

The Case II model corresponds to a diffusion process which depends on the relaxation of the PS matrix and it is independent of the concentration profile. The faster diffusing component, PVME, diffuses into the slower diffusing component, PS, and the original sharp interface moves into the slower moving component, PS, remaining as a sharp interface. The Case II diffusion is characterized by an interface velocity, K_i, which defines how fast the interface move into the PS layer. The cumulative concentration of PVME using the Case II model was derived previously [16] and is given by

$$Q_{II}(t) = c_{PV}^{eq}\exp\left[\frac{-2(\delta_1 - k_i t)}{d_p}\right] \quad (4)$$

where Q_{II} is the Case II component of the PVME cumulative concentration and c_{PV}^{eq} is the equilibrium concentration of PVME obtained from the experimental data at long diffusion times.

The PVME cumulative concentration may have both Fickian and Case II components. This can be taken into account by using a linear combination of the two cases as given by

$$Q(t) = (1 - \phi_{II})\,Q_F(t) + \phi_{II}\,Q_{II}(t) \quad (5)$$

where Q is the PVME cumulative concentration inside the penetration depth, Q_F and Q_{II} are the Fickian and Case II components of the cumulative concentration, respectively, and Φ_{II} is the fraction of the Case II component.

A typical cumulative concentration of PVME at 105 °C is shown in Fig. 4. The solid line is the best fit using Equation 5 with 20% and 80% Case II and Fickian components, respectively. The dotted lines 1 and 2 are the Case II and Fickian components of the best fit, respectively. The error bars were determined from the standard deviation of the intensity and linewidth of each ATR–FTIR peak based on a 95% confidence level. The maximum error in the values of PVME cumulative concentrations was 18%. Previous experimental results for diffusion at the PS–PVME interface showed that the diffusion profiles at 105 and 85 °C, corresponding to 5 °C above and 15 °C below the T_g of PS, had 20% and 70% Case II component, respectively. Therefore, all of the experimental data

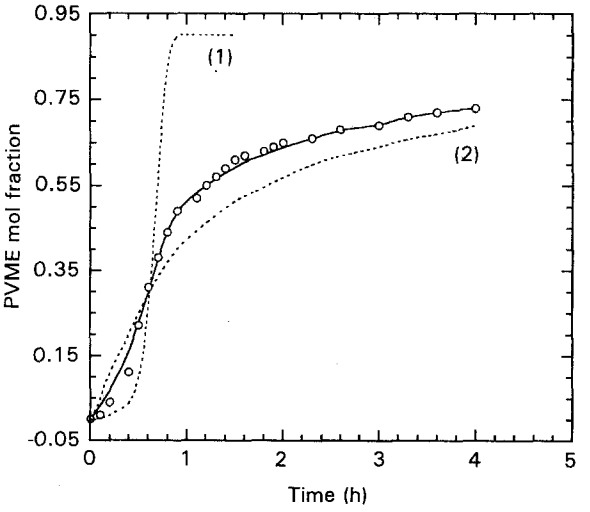

Figure 4 Comparison of the experimental mole fraction of PVME as a function of interdiffusion time and a combination of Fickian and Case II models using Equation 5 at 105 °C. (———) Best fit using Equation 5, (- - -) (1) Case-II and (2) Fickian components of the best fit, respectively. The PS and PVME $\overline{M_w}$ were 1.05×10^5 and 9.9×10^4 with polydispersity indices of 1.06 and 2.10, respectively. The PS film was spin cast on germanium crystal at 250 r.p.m. from a 5% *p*-xylene solution. The PVME film was spin cast on the PS film at 250 r.p.m. from a 10% isobutanol solution. The PS and PVME film thickness were 0.7 and 6.6 μm, respectively. The best fit to the experimental data was obtained with a diffusion coefficient of $1.1 \times 10^{-12}\,cm^2\,s^{-1}$, the interface velocity of $2.6 \times 10^{-8}\,cm\,s^{-1}$, and 70% Case II component.

measured at 105 and 85 °C were analysed with 20% and 70% Case II component, respectively.

4. Results and discussion

The T_g of PS and PVME blends were measured as a function of composition with DSC, as shown in Table II. All of the blends exhibited only one T_g. The T_g of the blends with 0/100, 50/50, 70/30, 80/20, 90/10, and 100/0 wt/wt PS/PVME were − 28, − 11, 38, 47, 66, and 102 °C, respectively, in excellent agreement with the values reported in the literature [21]. These results indicate that the PS–PVME blends are compatible for all compositions ranging from 0–100 wt % PS.

The thermal degradation of PVME and its blends with PS was studied by Park *et al.* [20] and they reported that water vapour and carbon dioxide were evolved during the thermal oxidation of PVME. Therefore, in our studies, TGA was used to study the degradation of PS–PVME blends by monitoring the weight loss as a function of composition and temperature. The composition dependence for the degradation of PS–PVME blends at 130 °C is shown in Fig. 5. According to this figure, PVME is the least stable compound in this blend and as PVME is added to a pure PS sample, the induction period for the degradation decreases from over 20 h to less than 24 h. The temperature dependence of the PVME thermal degradation is shown in Fig. 6. According to this figure, there is less than 0.2% weight loss of PVME for 4 h at 120 °C, 5 h at 110 °C, 14 h at 100 °C, and 20 h at 90 °C. Therefore, the duration of experiments at 85 and 105 °C was kept below 30 and 6 h, respectively, to

TABLE II Composition dependence of T_g for PS–PVME blends

PS (wt %)	T_g (°C)
0	− 28
50	− 11
70	38
80	47
90	66
100	102

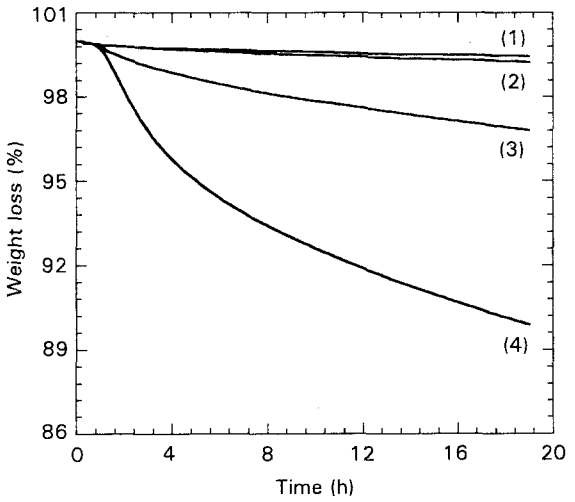

Figure 5 Per cent weight loss of PS–PVME blends at 130 °C as a function of time for (1) 100/0, (2) 80/20, (3) 60/40, and (4) 20/80 wt/wt PS/PVME, respectively. The $\overline{M_w}$ of PS and its polydispersity were 1.05×10^5 and 1.06, respectively. The $\overline{M_w}$ of PVME and its polydispersity were 9.9×10^4 and 2.1, respectively.

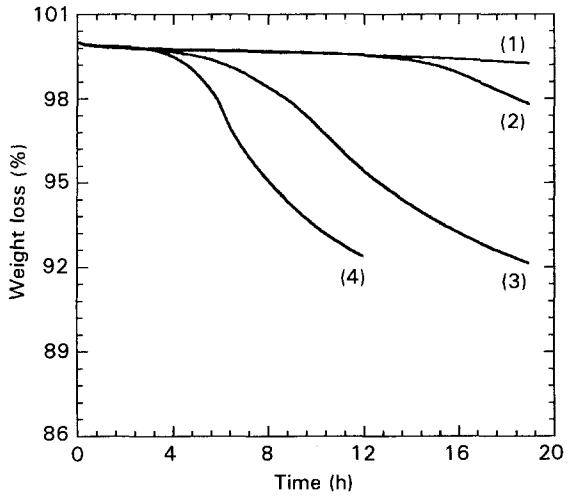

Figure 6 Per cent weight loss of PVME as a function of time at (1) 120 °C, (2) 110 °C, (3) 100 °C, and (4) 90 °C, respectively. The $\overline{M_w}$ of PVME and its polydispersity were 9.9×10^4 and 2.1, respectively.

ensure no degradation of PVME occurred during the experiment.

4.1. Time dependence of interdiffusion

The time dependence of interdiffusion at the PS–PVME interface was studied with PS films of different thickness. PS films were cast by spin coating from a 5% toluene or a *p*-xylene solution at 250 r.p.m. The thickness of the films were measured as a function of distance from the centre of the ATR crystal with profilometry and the results are shown in Fig. 7. According to this figure, the thickness of the PS films cast from *p*-xylene and toluene solution were 0.7 and 1.1 μm, respectively. The PVME film was spin coated directly on the PS film from a 10% solution of PVME in isobutanol at 250 r.p.m. The thickness of the PVME film was 6.6 μm.

The cumulative concentration of PVME as a function of time for the PS–PVME pair at 85 and 105 °C is compared in Fig. 8 for PS film thickness of 1.1 and 0.7 μm. According to this figure, at 85 °C corresponding to 15 °C below the T_g of PS, the shape of the PVME cumulative concentration curve changed and became more sigmoidal as the PS film thickness was

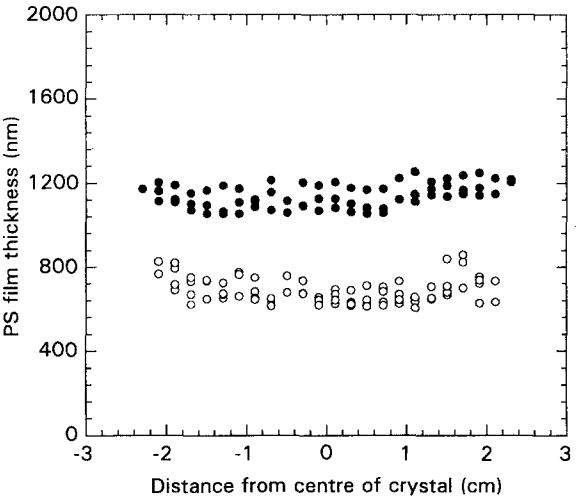

Figure 7 Thickness of PS film on a germanium crystal. The PS with $\overline{M_w}$ of 1.05×10^5 and polydispersity index of 1.06 was spin cast at 250 r.p.m. from (○) 5 wt% *p*-xylene or (●) toluene solutions.

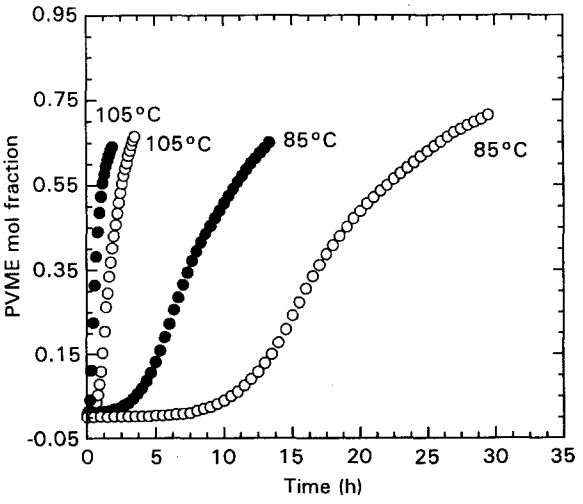

Figure 8 The effect of PS film thickness on PVME cumulative concentration at 85 and 105 °C versus interdiffusion time. The PS film thickness was (○) 0.7 μm and (●) 1.1 μm. The PS with $\overline{M_w}$ of 1.05×10^5 and polydispersity index of 1.06 was spin cast at 250 r.p.m from a 5% toluene or *p*-xylene solution. The PVME with $\overline{M_w}$ of 9.9×10^4 and polydispersity index of 2.10 had a film thickness of 6.6 μm.

increased. The independent variable time can be made dimensionless with respect to the PS film thickness by

$$t^* = \frac{tD_{PV}}{\delta_1} \quad (6)$$

where t^* is the dimensionless time, D_{PV} is the self-diffusion coefficient of PVME, and δ_1 is the thickness of the PS layer.

If the diffusion coefficient is independent of time, the PVME cumulative concentrations with different PS film thickness should be superimposed when plotted against dimensionless time. The cumulative concentrations in Fig. 8 are replotted versus dimensionless time in Fig. 9. At 105 °C, the cumulative concentrations for the two PS film thickness superimpose except toward the end of the diffusion process. On the other hand, at 85 °C corresponding to 15 °C below the T_g of PS, the cumulative concentrations do not superimpose indicating that the diffusion coefficient is time dependent. This is in good agreement with our previous results that the PVME cumulative concentrations at 105 and 85 °C had 20% and 70% non-Fickian component, respectively. This indicates that the PS matrix changes significantly as interdiffusion proceeds giving rise to time-dependent interdiffusion coefficient.

The relaxation times of PS and PVME chains were previously determined by us [17] using the following equation derived from the reptation model for the relaxation of a polymer chain in the melt

$$\tau_{rep} = \left(\frac{48}{5}\right)\left(\frac{L^2}{\pi^2 RT}\right)\left(\frac{M_e^2}{\rho b^2 M_0}\right)\eta_0 \quad (7)$$

where τ_{rep} is the relaxation time of a chain using reptation theory, L is the contour length of a polymer chain, R is the gas constant, T is temperature, M_e is the entanglement molecular weight, M_0 is the repeating unit molecular weight, ρ is the polymer density, b is the statistical segment length, and η_0 is the zero shear viscosity of the polymer which is temperature dependent.

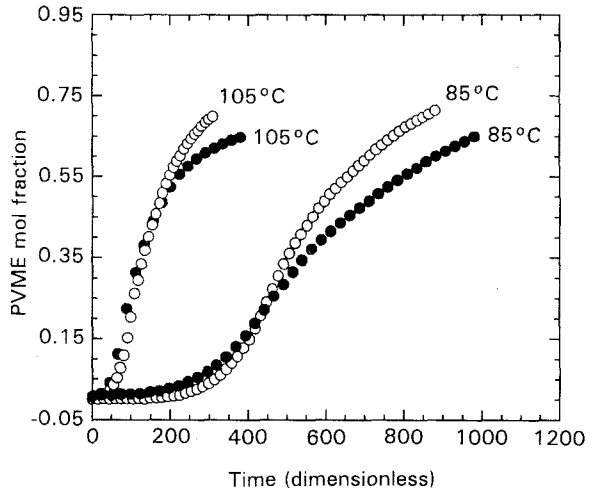

Figure 9 The effect of PS film thickness on PVME cumulative concentration at 85 and 105 °C versus dimensionless time. The dimensionless time is defined by Equation 6. The PS film thickness was (○) 0.7 μm or (●) 1.1 μm. The PS with $\overline{M_w}$ of 1.05×10^5 and polydispersity index of 1.06 was spin cast at 250 r.p.m. from a 5% toluene or *p*-xylene solution. The PVME with $\overline{M_w}$ of 9.9×10^4 and polydispersity index of 2.10 had a film thickness of 6.6 μm.

In order for PVME to swell the PS matrix, the relaxation time of the PVME should be compared with the PS relaxation time corresponding to the critical molecular weight for entanglement. Using the above equation, the relaxation times of PVME and PS at 105 °C are 0.3 and 8 s, respectively, with the PS relaxation time an order of magnitude greater than the PVME. On the other hand, at 85 °C, the relaxation times of PVME and PS are 0.7 and 110 s, respectively, with the PS relaxation time more than two orders of magnitude greater than PVME. This indicates that at 105 °C as well as 85 °C the diffusion process is partially controlled by the relaxation of the PS matrix, giving rise to a time-dependent diffusion coefficient. The best fit parameters to the PVME cumulative concentrations using a combination of Fickian and Case II models at 85 and 105 °C for PS film thickness of 0.7 and 1.1 μm is given in Table III. The best fit for the data at 105 and 85 °C was obtained with 20% and 70% non-Fickian component, respectively.

4.2. Effect of PS MW and MWD

PS films with molecular weights of 1.05×10^5, 8.5×10^5, and 3×10^6 were spin coated on ATR crystals from *p*-xylene solution at 250 r.p.m. with concentrations of 5.0, 2.5, and 1.5 wt % PS, respectively. The polydispersity of the PS samples was less than 1.06. The thickness of PS films, measured by profilometry, was 0.7, 0.55, and 0.45 μm for PS molecular weights of 1.05×10^5, 8.5×10^5, and 3×10^6, respectively.

The effect of PS molecular weight on the PVME cumulative concentration as a function of dimensionless time at 105 and 85 °C is shown in Figs 10 and 11, respectively. According to these figures, the rate of diffusion of PVME in PS decreases slightly at 105 °C and is independent of PS molecular weight at 85 °C as the PS molecular weight increases from 1.05×10^5 to 3.0×10^6. This indicates that at 105 °C, PS as well as PVME diffuses across the interface, whereas at 85 °C, interdiffusion is limited by the rate of swelling of PS by PVME. The data in Figs 10 and 11 are analysed using a combination of Fickian and Case II models and the results are given in Table IV. The interface velocities in Table IV are a measure of the rate of swelling of PS by PVME and are independent of the molecular weight. At 105 °C, the diffusion coefficient is related to molecular weight by $M^{-0.4}$ and at 85 °C, it is independent of molecular weight. This indicates that the

TABLE III Effect of PS film thickness on interdiffusion at the interface between PS and PVME at 85 and 105 °C

PS film thickness, δ_1 (μm)	Interface velocity, K_i		Diffusion coefficient, D	
	(10^8 cm s^{-1})(10^9 cm s^{-1})		(10^{12} cm^2 s^{-1})	(10^{15} cm^2 s^{-1})
	105 °C	85 °C	105 °C	85 °C
0.7	2.6	2.2	1.0	8.8
1.1	1.5	1.7	1.2	2.4

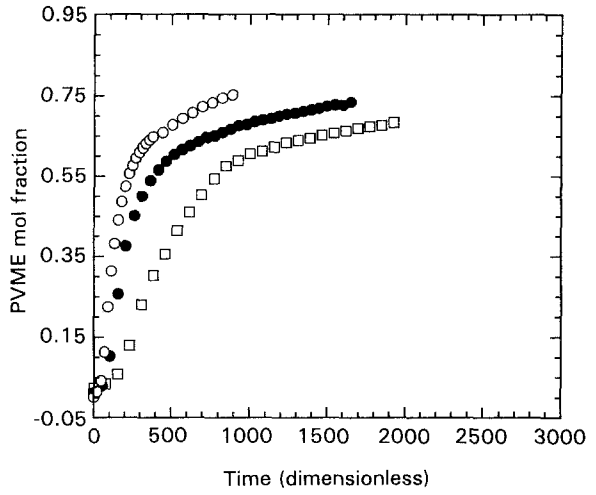

Figure 10 The effect of PS molecular weight on PVME cumulative concentration at 105 °C versus dimensionless time. The dimensionless time is defined by Equation 6. The monodisperse PS $\overline{M_w}$ were (○) 1.05×10^5, (●) 8.5×10^5, and (□) 3.0×10^6 with film thickness of 0.7, 0.55, and 0.45 μm, respectively. The PVME film thickness was 6.6 μm.

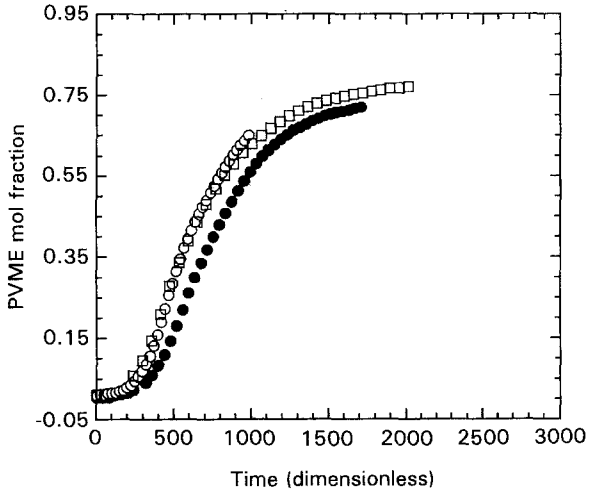

Figure 11 The effect of PS molecular weight on PVME cumulative concentration at 85 °C versus dimensionless time. The dimensionless time is defined by Equation 6. The monodisperse PS $\overline{M_w}$ were (○) 1.05×10^5, (●) 8.5×10^5, and (□) 3.0×10^6 with film thickness of 0.7, 0.55, and 0.45 μm, respectively. The PVME film thickness was 6.6 μm.

interdiffusion process is independent of molecular weight of the slower diffusing component, PS. According to the fast-mode theory, proposed by Kramer *et al.* [22] and Sillescu [23] for polymers with different molecular weights, and extended by us to dissimilar polymer interfaces [24], interdiffusion is independent of the molecular weight of the slow-diffusing component. The results in Table IV are in good agreement with the fast-mode theory.

The effect of PS polydispersity on the PVME cumulative concentration was studied using trimodal distributions constructed from monodisperse PS samples. The weight average molecular weight of all the samples was 1.05×10^5 with polydispersity indices of 1.06, 2, and 3. The trimodal distributions were constructed from samples with $\overline{M_w}$ of 1.5×10^4 (PSI), 1.05×10^5 (PS2), and 4.7×10^5 (PS3) with PI values of less than 1.06 for all the samples. It should be noted that the molecular weight of PS1 is below the entanglement molecular weight and PS2 and PS3 are above the entanglement molecular weight. The weight percent of monodisperse polymers for constructing polydisperse samples are given in Table I.

The time dependence of the cumulative concentration of PVME for PS polydispersities of 1.06, 2.0, and 3.0 at 85 °C is shown in Fig. 12. As the PS polydispersity index increases, the rate of diffusion of PVME in PS also increases. The data in Fig. 12 are analysed with a combination of Fickian and Case II models and the results are shown in Table V. According to this table, the interface velocity as well as the diffusion coefficient increases with polydispersity, indicating that the relaxation time of the PS chains, as well as the diffusive properties of the PS matrix, change with polydispersity. The diffusion of PVME in polydisperse PS matrix can be analysed in terms of a binary PS matrix with one below and the other above the entanglement molecular weight. Diffusion in these systems is controlled by the higher molecular weight component which is the rate-limiting step.

The component with $\overline{M_w}$ below the entanglement molecular weight is PS1 with molecular weight $M_{w,1}$ and weight fraction w_1. The component with $\overline{M_w}$ above the entanglement is PS23 with molecular weight $M_{w,23}$ which is $(w_2M_{w,2} + w_3M_{w,3})/(w_2 + w_3)$ and weight fraction $w_{2,3}$ equal to $(w_2 + w_3)$. The critical entanglement molecular weight for PS, M_e^0, is 1.8×10^4 [25]. The diffusion of PS23 chains in PS blends with $M_{w,23} \gg M_{w,1} \approx M_e^0$ has been studied by Green and Kramer [26] who showed that $D_{2,3} \propto M_{w,1}^{-1} M_{w,2}^{-0.5}$ and by Antonietti *et al.* [27] who showed that $D_{2,3} \propto M_{w,1}^{-a} M_{w,2}^{-1}$ with a somewhat larger than unity. These studies show that the presence of the PS1 chains contributes significantly to the Stokes–Einstein diffusion of the higher molecular weight component, PS23.

TABLE IV Effect of PS molecular weight on interdiffusion at the interface between PS and PVME at 85 and 105 °C

PS Molecular weight, M_w	Interface velocity, K_i		Diffusion coefficient, D	
(10^{-3} g mol^{-1})	(10^8 cm s^{-1}) 105 °C	(10^9 cm s^{-1}) 85 °C	(10^{12} cm^2 s^{-1}) 105 °C	(10^{15} cm^2 s^{-1}) 85 °C
105	2.6	2.2	1.0	8.8
850	2.2	2.1	0.5	8.8
3000	1.0	3.1	0.2	13.6

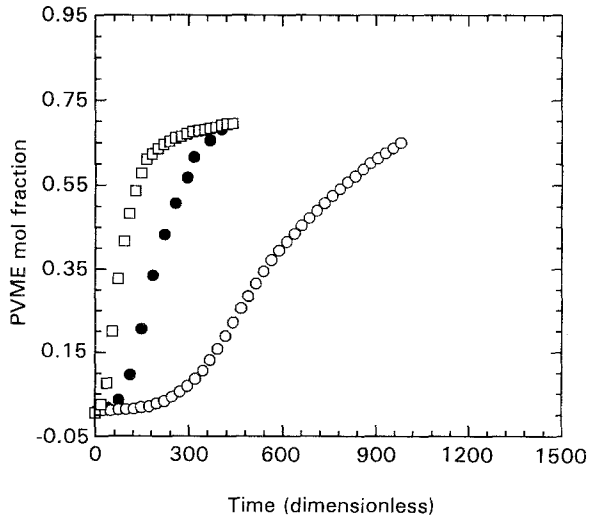

Figure 12 The effect of PS molecular weight distribution on PVME cumulative concentration at 85 °C versus dimensionless time. The dimensionless time is defined by Equation 6. The polydispersity indices of the PS samples were (○) 1.06, (●) 2.0, and (□) 3.0. The PS and PVME film thickness were 0.7 and 6.6 μm, respectively.

TABLE V Effect of PS molecular weight distribution on interdiffusion at the interface between PS and PVME at 85 °C

PS polydispersity index PI	Interface velocity K_i (10^9 cm s^{-1})	Diffusion coefficient D (10^{15} cm^2 s^{-1})
1.1	2.2	8.8
2.0	6.1	27.5
3.0	14.6	55.0

The diffusion coefficient of the higher molecular weight component is also a function of the effective entanglement spacing of the PS23 chains, $M_{e,23}$ which is the same as the critical entanglement molecular weight for a PS matrix consisting only of PS23 chains and in the presence of PS1 chains is given by [28, 29]

$$M_{e,23} = M_e^0/w_{23} \quad (8)$$

In the reptation [30], constraint release [31], and tube renewal [32] mechanisms for diffusion in polymer melts, the diffusion coefficient is related to the effective entanglement spacing by $M_{e,23}^1$, $M_{e,23}^{1.5}$, and $M_{e,23}^3$, respectively. Using Equation 8, the diffusion coefficient of the higher molecular weight PS component is related to PS23 weight fraction, w_{23}, by

$$D_{23} = w_{23}^{-1} \text{ (reptation)} \quad (9)$$

$$D_{23} = w_{23}^{-1.5} \text{ (constraint release)} \quad (10)$$

$$D_{23} = w_{23}^{-3} \text{ (tube renewal)} \quad (11)$$

The PS samples with polydispersity indices of 1.06, 2, and 3 contain 100, 83.3, and 65.6 wt % higher molecular weight PS23 component, respectively, as given in Table I. The experimental diffusion coefficients as a function of polydispersity, presented in Table V, are related to the weight fraction of PS23 component by $w_{23}^{-2.9}$, indicating that the tube renewal mechanism contributes significantly to the relaxation of PS chains and the diffusion process at the interface.

4.3. Effect of PVME MW

The effect of PVME molecular weight was studied by fractionating three times the original PVME sample from water solution. After fractionation, the PVME $\overline{M_w}$ increased to 1.7×10^5 and the polydispersity index reduced to 1.4. The time dependence of the PVME cumulative concentration for the two PVME samples at 85 and 105 °C is shown in Fig. 13. According to this figure, as the PVME $\overline{M_w}$ increases from 9.9×10^4 to 1.7×10^5, the rate of swelling of PS by PVME decreases significantly. Comparison of the results for PS molecular weight effect shown in Figs 10 and 11 with results in Fig. 13 indicates that interdiffusion at the interface of PS and PVME is dominated by the faster diffusing component, PVME.

The diffusion coefficient and interface velocity were calculated from the experimental data and the results are given in Table VI. The best fit at 85 and 105 °C were obtained with 70% and 20% non-Fickian component, respectively. At 85 and 105 °C the diffusion coefficient is related to PVME molecular weight by $M_{w,PV}^{-1.1}$ and $M_{w,PV}^{-1.3}$, respectively. These results are in good agreement with the fast-mode theory in which the interdiffusion coefficient is inversely related to the molecular weight of the faster diffusing component, PVME.

5. Conclusions

The time dependence of interdiffusion at the interface between PS and PVME and the effect of PS and PVME molecular weight and molecular weight distribution were investigated with attenuated total reflection infrared spectroscopy (ATR–FTIR) below

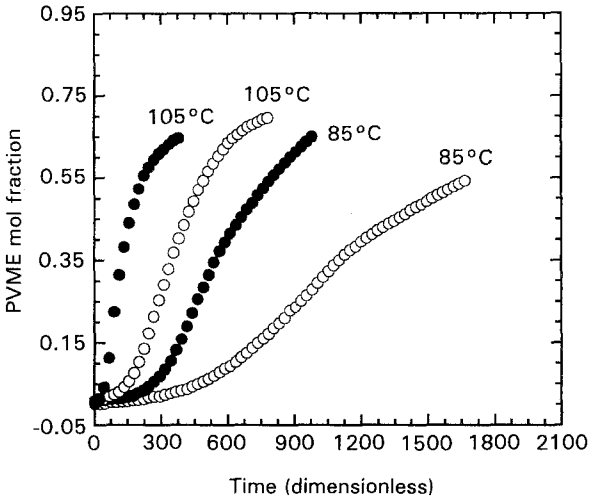

Figure 13 The effect of PVME molecular weight on PVME cumulative concentration at 85 and 105 °C versus dimensionless time. The dimensionless time is defined by Equation 6. The PVME $\overline{M_w}$ before and after fractionation were (●) 9.9×10^4 and (○) 1.7×10^5 with polydispersity indices of 2.1 and 1.4, respectively. The thickness of the PVME films were 6.6 μm. The PS with $\overline{M_w}$ of 1.05×10^5 and polydispersity index of 1.06 had a film thickness of 0.7 μm.

TABLE VI Effect of PVME molecular weight on interdiffusion at the interface between PS and PVME at 85 and 105 °C

PVME molecular weight, M_w	Interface velocity, K_i		Diffusion coefficient, D	
(10^{-3} g mol^{-1})	(10^{8} cm s^{-1}) 105 °C	(10^{9} cm s^{-1}) 85 °C	(10^{12} cm^2 s^{-1}) 105 °C	(10^{15} cm^2 s^{-1}) 85 °C
99	2.6	2.2	1.0	8.8
120	0.8	1.1	0.5	5.0

and above the T_g of PS. At 105 and 85 °C, the diffusion process was partially controlled by the relaxation time of the PS matrix, giving rise to a time-dependent diffusion coefficient. The interdiffusion coefficient was independent of PS molecular weight but strongly dependent on PVME molecular weight in good agreement with the fast-mode theory in which interdiffusion is controlled by the faster moving component. The molecular weight distribution of PS significantly affected the interdiffusion process. It was shown that the diffusion coefficient was related to the weight fraction of the higher molecular weight PS component by $w_{23}^{-2.9}$. This indicated that tube renewal significantly affects the relaxation of PS chains as the low molecular weight component is added to the matrix.

Acknowledgements

This work was supported by National Institute of Health (NIH) grant GM45027; the ATR–FTIR spectrometer was purchased with a National Science Foundation (NSF) grant CTS-90-07141. We thank Loy Tay for substantial technical assistance for DSC and TGA studies.

References

1. K. JUD, H. H. KAUSCH and J. G. WILLIAMS, *J. Mater. Sci.* **16** (1981) 204.
2. H. W. KAMMER, *Acta. Polym.* **34** (1983) 112.
3. W. H. PRITCHARD, *Aspects Adhesion* **6** (1971) 12.
4. W. D. BASCOM, *Adv. Polym. Sci.* **85** (1988) 89.
5. S. S. VOYUTSKII, *J. Adhesion* **3** (1971) 69.
6. S. S. VOYUTSKII, "Autohesion and Adhesion of High Polymers" (Wiley, New York, 1963).
7. E. H. ANDREWS, *J. Polym. Sci. Polym. Symp. Edn* **72** (1985) 295.
8. A. N. GENT and C. W. LIN, *J. Adhesion* **32** (1990) 113.
9. P. G. de GENNES, *C. R. Acad. Sci. Paris, Serie II* **292** (1981) 1505.
10. A. KARIM, G. P. FELCHER and T. P. RUSSELL, *Polym. Prepr.* **31(2)** (1990) 69.
11. P. J. MILLS, P. F. GREEN, C. J. PALMSTROM, J. W. MAYER and E. J. KRAMER, *Appl. Phys. Lett.* **45** (1984) 957.
12. E. J. KRAMER, P. F. GREEN and C. J. PALMSTROM, *Polymer* **25** (1984) 473.
13. S. J. WHITLOW and R. P. WOOL, *Macromolecules* **22** (1989) 2648.
14. F. BRUDER and R. BRENN, *ibid.* **24** (1991) 5552.
15. B. B. SAUER and D. J. WALSH, *ibid.* **24** (1991) 5948.
16. E. JABBARI and N. A. PEPPAS, *ibid.* **26** (1993) 2175.
17. *Idem, J. Adhesion*, submitted.
18. A. A. GORBUNOV, A. M. SKVORTSOV and M. B. TENNIKOV, *Vysokomol. Soyed.* **A31** (1989) 1306.
19. N. J. HARRICK, "Internal Reflection Spectroscopy" (Wiley, New York, 1967).
20. H. PARK, E. M. PEARCE and T. K. KWEI, *Macromolecules* **23** (1990) 434.
21. H. YANG, M. SHIBAYAMA, R. S. STEIN, N. SHIMIZU and T. HASHIMOTO, *ibid.* **19** (1986) 1667.
22. E. J. KRAMER, P. F. GREEN and C. J. PALMSTROM, *Polymer* **25** (1984) 473.
23. H. SILLESCU, *Makromol. Chem. Rapid Commun.* **8** (1987) 393.
24. E. JABBARI and N. A. PEPPAS, *Polymer*, in press.
25. D. W. van KREVELEN, "Properties of Polymers" (Elsevier, New York, 1990).
26. P. F. GREEN and E. J. KRAMER, *Macromolecules* **19** (1986) 1108.
27. M. ANTONIETTI, J. COUTANDIN and H. SILLESCU, *ibid.* **19** (1986) 793.
28. H. WATANABE and T. KOTAKA, *ibid.* **20** (1987) 530.
29. *Idem ibid.* **20** (1987) 535.
30. P. G. de GENNES, *J. Chem. Phys.* **55** (1971) 572.
31. J. KLEIN, *Macromolecules* **19** (1986) 105.
32. W. W. GRAESSLEY, *Adv. Polym. Sci.* **47** (1982) 67.

Received 11 June 1993
and accepted 19 January 1994